INSTITUT DE FRANCE
Académie des sciences

Comptes Rendus

Mécanique

Ayoub Mbarek, Alfonso Fernández, Ahmed Hammami, Fakher Chaari, Fernando Viadero and Mohamed Haddar

Operational modal analysis using order-based analysis in a two-stage planetary gear with mechanical power recirculation

Volume 350 (2022), p. 391-411

Published online: 28 July 2022

https://doi.org/10.5802/crmeca.123

Les Comptes Rendus. Mécanique *sont membres du Centre Mersenne pour l'édition scientifique ouverte*
www.centre-mersenne.org
e-ISSN : 1873-7234

Comptes Rendus
Mécanique
2022, Vol. 350, p. 391-411
https://doi.org/10.5802/crmeca.123

Short paper / *Note*

Operational modal analysis using order-based analysis in a two-stage planetary gear with mechanical power recirculation

Ayoub Mbarek [a, b], **Alfonso Fernández** [b], **Ahmed Hammami** [a], **Fakher Chaari** [*, a], **Fernando Viadero** [b] **and Mohamed Haddar** [a]

[a] Mechanics, Modelling and Production Laboratory, National School of Engineers Sfax, Tunisia

[b] Department of Structural and Mechanical Engineering, Faculty of Industrial and Telecommunications Engineering, University of Cantabria, Santander, Spain

E-mails: ayoubmbarekenit@gmail.com (A. Mbarek), alfonso.fernandez@unican.es (A. Fernández), ahmed.hammami2109@gmail.com (A. Hammami), fakher.chaari@gmail.com (F. Chaari), fernando.viadero@unican.es (F. Viadero), mohamed.haddar2016@gmail.com (M. Haddar)

Abstract. Modal analysis techniques are considered as the most used of techniques allowing the characterization of the dynamic behaviour in systems such as planetary gear transmission. During operational conditions, the modal behaviour can be altered. The main purpose of this paper is to estimate the Modal Properties (MP) of two-stage planetary gear during non-stationary regimes using a further version of Operational Modal Analysis (OMA). The natural frequencies and modal damping are determined by Order Tracking (OT) and processed using diagram stability tool. Moreover, the modelling and the treatment of the non-stationary regimes were established. The proposed technique proves that order-based OMA can extract resonances which are related to the interaction between structural modes and the rotational speed harmonics. The experimental measurements are compared to the obtained results via a numerical model. It proves that the natural frequencies and modal damping are significantly dependent on the load.

Keywords. Planetary gear, Non-stationary regimes, OMA, Natural frequencies, Modal damping.

Manuscript received 1 October 2021, revised 1 July 2022, accepted 4 July 2022.

1. Introduction

Planetary gear systems are powerful mechanisms in the transmission system. They are characterized by a high ability to work under both stationary and non-stationary regimes. However, these systems suffer typically from some drawbacks like noise or vibration, especially when they run

* Corresponding author.

close to the critical resonant frequencies and other Modal Properties (MP). Only a limited number of literature reviews have dealt with MP identification techniques, the characteristics of each method, their main advantages, and their limitations.

The modal testing is usually recommended as a complementary tool for the conception, validation, and fault diagnosis [1]. Therefore, different methods were developed to identify the MP in such static or dynamic conditions such as the Conventional Modal Analysis and the Operational Modal Analysis (OMA) [2–4]. On the one hand, the conventional technique is based on exciting the structures in a static condition. It ruled out some dynamic characteristics like the velocity function or the harmonic component. This method is carried out to recover the response function frequency and estimate the MP [5]. Nevertheless, the conventional method does not apply to the gearbox system since it excludes the meshing functions. On the other hand, the Operational method is applicable when the system is excited in a stationary regime.

Furthermore, several researchers proposed other approaches. Provasi *et al.* [6] investigated MP using Kalman filter. This approach allows the identification of the modal function even when it is associated with multiple inputs such as force and velocity. The application of this modal implies some knowledge of operational forces. Other researchers like Mohanty and Rixen [7–10] and Kordkheili [11] used time-domain approaches, where the rectification of the basic identification methods was reported. The work of Modak [12, 13] used a random approach to suppress the noise amplitude in case of OMA. Specifically, this method tracks the periodic and noisy signals. To estimate MP, Peeters *et al.* [14] developed a new version of Least Squares Complex Exponential (LSCE) called Polymax. This method is characterized by a benchmark to select the model order with well-structured system poles.

To identify the dynamic characteristics, different methods use stationary conditions i.e. constant load and speed. However, in case of non-stationary condition, when the frequency is directly related to time, different approaches were required to consider these regimes. To study this case, Haykin *et al.* [15], proposed the Order Tracking (OT) method to identify the amplitudes of order. The use of this method is linked to the knowledge and theories related to the vibration signal and frequency characteristics represented in the velocity function. According to [16–18], the harmonic components from the obtained signals are defined by the Vold–Kalman filter. In the work of Wu [19], the OT technique was developed to carry out a defect diagnosis in a gear system. The developed method analyses the evolution of the order function amplitude in case of machine monitoring. The collected signals were compared to the Recursive Least-Squares (RLS) filtering algorithm. Recently, Yang *et al.* [20] developed a Particle Swarm Optimization algorithm to study the power spectrum MP of the obtained signal while the machine is running. Their experimental and numerical results are correlated.

Mbarek *et al.* [4] reported three types of modal analysis techniques. It shows that the Order-Based Modal Analysis (OBMA) could be an efficient technique to extract MP in non-stationary operating condition. However, the MP sensitivity to the load was investigated. Ericson and Parker [21] reported the influence of the external torque, bearing dependent load and Mesh Stiffness Function (MSF) on the dynamic behaviour and MP system. Their experimental results were compared with those issued from analytical and finite element model. In the Mbarek *et al.* [22] study, the impact of the torque and MSF variation on the MP was analysed using a lumped mass model of a two-stage planetary gear characterised by 72 Degrees of Freedom (DOF). To this end, the conventional modal analysis technique was adopted to identify the natural frequency. Despite the variety of the cited studies, the loading effects on MP under non-stationary operation are scarce if not totally missing in the literature.

In this work, a further version of OMA using order-based techniques is investigated. This approach has a big potential in the industrial engineering area and specially for condition monitoring. In fact, it allows not only the identification of the MP but also the study of the parameters

that influence the systems behaviour under different operational conditions using sensors and a data acquisition system. In fact, these systems present a non-linearity to the externally applied torque. So, the influence of specific parameters such as load could be investigated.

The obtained signals are compared to others acquired theoretically using the concentrated mass model, which is developed to provide further insight into the dynamic characteristic of the system. The model was driven in the run-up regime where the MSF fluctuation was considered. Besides, the impact of the torque on the dynamic behaviour was analysed using time response and the Short Time Fourier Transform (STFT) analysis. Then, the angle-domain OT method was formulated and implemented to determine the order function. Finally, the system MP presented by the natural frequencies and modal damping was examined highlighting the MP sensitivity to the load.

2. Processing method

An STFT spectrogram was adapted to process the experimental and numerical time signals to track the speed variation for each level of load. The spectrogram gives a clue about the Gear Mesh Frequency (GMF) harmonics. The Hamming window was implemented with a frequency resolution of 2 Hz/line.

The signals issued from the tachometer and the accelerometers were recorded using the LMS SCADAS 316 Data Acquisition System and analysed using the LMS Test Lab 15A software.

The most important order was estimated via the angle-domain method. In addition, the MP for each torque case was estimated via a Stabilization diagram. More details on the OT and MP extraction are detailed in the literature [23].

The measurements were collected in timeframe. To transform them to the angular domain, a reference signal was used to determine the time increment characterized by spaced angular intervals. Usually, the tachometer signal is used for this issue, in our case, the tachometer is used, and it is mounted on the input shaft.

The Fourier transform kernels are computed according to (1) and (2):

$$\boldsymbol{a_n} = \frac{\mathbf{1}}{\boldsymbol{N}} \sum_{\boldsymbol{n=1}}^{\boldsymbol{N}} \boldsymbol{x}(\boldsymbol{n}\Delta\boldsymbol{\theta})\cos(\mathbf{2}\boldsymbol{\pi o_m n}\Delta\boldsymbol{\theta}) \tag{1}$$

$$\boldsymbol{b_n} = \frac{\mathbf{1}}{\boldsymbol{N}} \sum_{\boldsymbol{n=1}}^{\boldsymbol{N}} \boldsymbol{x}(\boldsymbol{n}\Delta\boldsymbol{\theta})\sin(\mathbf{2}\boldsymbol{\pi o_m n}\Delta\boldsymbol{\theta}), \tag{2}$$

where $\boldsymbol{o_m}$ denotes the order, which will be analysed later.

3. Order-based modal analysis

This method is highly recommended for rotating machinery as it combines the OMA method and the OT method.

Indeed, the OBMA is based on periodic excitation to obtain the machinery dynamic behaviours. Therefore, its applicable condition is that the mechanical system generates a periodic excitation force during the operational process. In fact, it generates a periodic excitation force whose frequency is proportional to the rotational speed during the revolution. OBMA aims to identify MP from the simulated or measured signal with crossing order. First, the system is excited in non-stationary regimes (run-up, run-down) [24]. Then, the OT method based on the filter method is used to extract a harmonic response known as engine orders. Finally, the MP is estimated using the stabilisation diagram (Figure 1) and the modal estimation method [4].

The proposed method is a further version of OMA, and is based on the exciting mode when the system runs in non-stationary condition, and it is well suited to the gear system. These systems

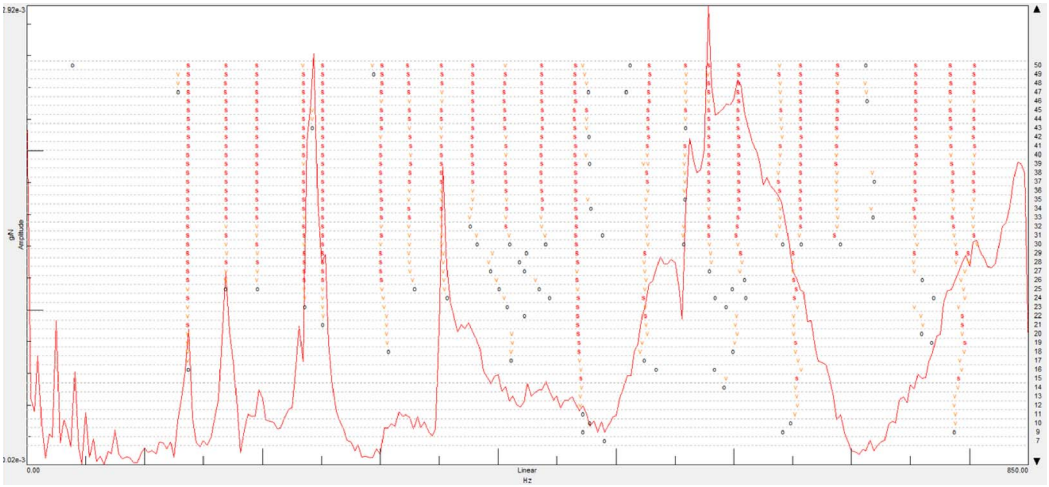

Figure 1. Stabilization diagram.

are working widely in non-stationary conditions. The proposed method was used previously by the authors and compared to the traditional modal analysis, the results obtained for both methods are very close, the main advantages of this method is its ability to estimate modal parameter when the system is in service, meaning that all influencing functions such as mesh stiffness and external excitation are present. The other approach or method has some limitations compared to the traditional modal analysis. The latter uses artificial excitation and the system is under static condition. Also, the basic version of OMA suffers from the end-order phenomena, and in this case several modes cannot be estimated.

The relationship between the system MP and order is explained by assuming the structure to be excited by a rotating mass with an increasing frequency [12]. Two perpendicular forces of equal amplitude [25], can represent it. The measured response $\boldsymbol{Y}(\boldsymbol{\omega})$ in the frequency domain is:

$$\boldsymbol{Y}(\boldsymbol{\omega}) = \boldsymbol{H}_{(:,\boldsymbol{f_x})}(\boldsymbol{\omega})\boldsymbol{F_x}(\boldsymbol{\omega}) + \boldsymbol{H}_{(:,\boldsymbol{f_y})}(\boldsymbol{\omega})\boldsymbol{F_y}(\boldsymbol{\omega}), \tag{3}$$

where $\boldsymbol{F}$ is for the force and $\boldsymbol{H}$ is the transfer function matrix.

If we consider the relationship between the two correlated forces, the response of the structure can be expressed as follows:

$$\boldsymbol{Y}(\boldsymbol{\omega})\mu\boldsymbol{\omega_0^2}(\boldsymbol{H}_{(:,\boldsymbol{f_x})}(\boldsymbol{\omega}) - \boldsymbol{j}\boldsymbol{H}_{(:,\boldsymbol{f_y})}(\boldsymbol{\omega}))\boldsymbol{\delta}(\boldsymbol{\omega} - \boldsymbol{\omega_0}), \tag{4}$$

where $\boldsymbol{\omega_0}$ denotes the rotational speed. From this equation, it seems that the measured output is proportional to the squared rotational speed and to a complex combination of the two structural FRFs related to $\boldsymbol{x}$ and $\boldsymbol{y}$ excitation. A structural FRF can be reformulated as shown below:

$$(\boldsymbol{H}_{(:,\bullet)})(\boldsymbol{\omega}) = \boldsymbol{V}(\boldsymbol{j\omega I} - \boldsymbol{j\Lambda})^{-1}\boldsymbol{L_\bullet} + \frac{\boldsymbol{1}}{\boldsymbol{\omega^2}}\boldsymbol{LR_\bullet} + \boldsymbol{UR_\bullet} \tag{5}$$

$\boldsymbol{V}$ and $\boldsymbol{\Lambda}$ are the modal shapes matrix and the modal poles matrix, respectively. $\boldsymbol{L}$ is the modal participation factor. The parameters $\boldsymbol{V}$, $\boldsymbol{\Lambda}$, $\boldsymbol{L}$ are the complex-valued MP, $\boldsymbol{LR_\bullet}$ and $\boldsymbol{UR_\bullet}$ are the real-valued lower and upper residuals, modelling the influences of the modes outside the considered frequency band. By inserting this modal decomposition, Equation (4) combined with (5) can be written as [25]:

$$\boldsymbol{Y}(\boldsymbol{\omega})\mu\boldsymbol{\omega^2}(\boldsymbol{V}(\boldsymbol{j\omega I} - \boldsymbol{j\Lambda})^{-1}(\boldsymbol{L_x} - \boldsymbol{jL_y}) + \frac{\boldsymbol{1}}{\boldsymbol{\omega^2}}(\boldsymbol{LR_x} - \boldsymbol{jLR_y}) + (\boldsymbol{UR_x} - \boldsymbol{jUR_y})). \tag{6}$$

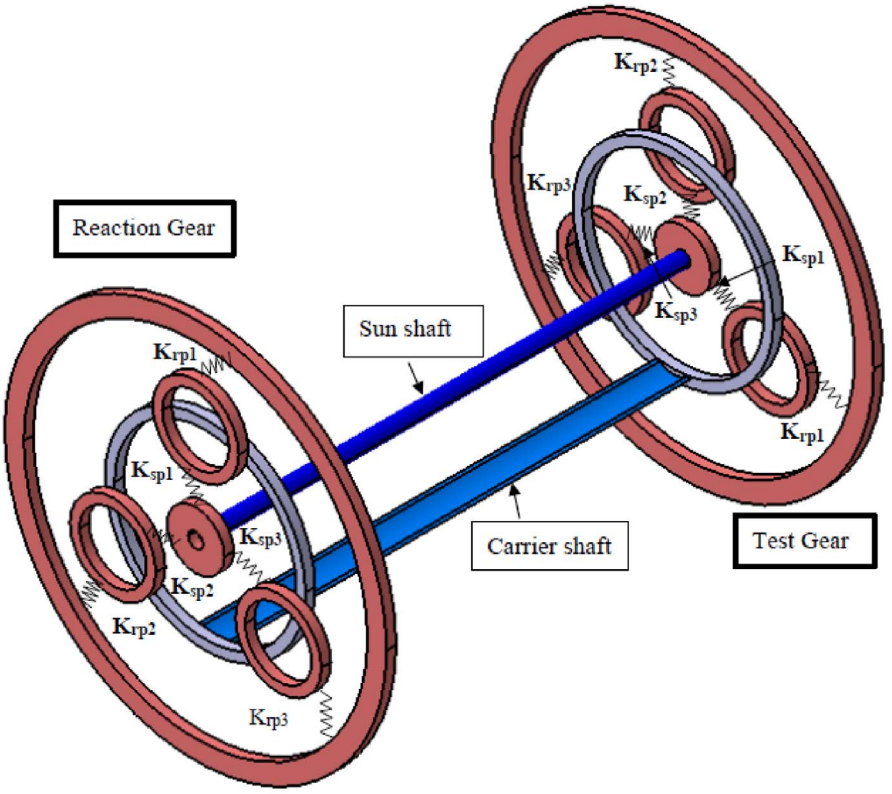

Figure 2. Planetary gear structure.

In the OBMA, the order functions are the transfer functions; they are sensitive to the input excitation and the response. In fact, in the studied cases, the transfer functions are obtained for a different measured response. These functions varied with the loading condition and so on the real physical pole as mentioned in equation. For this reason, the impact of the torque was discussed.

4. Numerical model

To analyse the system dynamic behaviour, a lumped model was used. It is a 72 DOF three-dimensional model characterised by six DOF per element. The two planetary sets are identical, only one stage is presented in Figure 2.

The carrier (c), ring (r), sun (s) and the three planets ($\boldsymbol{p1}, \boldsymbol{p2}, \boldsymbol{p3}$) are the main components, they are simulated as rigid bodies with mass $\boldsymbol{m_{ij}}$ and inertia $\boldsymbol{I_{ij}}$.

The bearings are modelled by a rigid spring with stiffness $\boldsymbol{K_{bix}}$, $\boldsymbol{K_{biy}}$, $\boldsymbol{K_{biz}}$, $\boldsymbol{K_{bi\Phi}}$, $\boldsymbol{K_{bi\Psi}}$ and $\boldsymbol{K_{bi\theta}}$ where ($\boldsymbol{i} = \boldsymbol{c}, \boldsymbol{r}, \boldsymbol{s}, \boldsymbol{p1}, \boldsymbol{p2}, \boldsymbol{p3}; \boldsymbol{j} = \boldsymbol{r}, \boldsymbol{t}$ and $\boldsymbol{x}, \boldsymbol{y}, \boldsymbol{z}, \boldsymbol{\Phi}, \boldsymbol{\Psi}, \boldsymbol{\theta}$) are the directions.

Both planetary gear sets are coupled with sun's and carrier's shaft. More details on the numerical model are listed in Mbarek *et al.* [4].

The analytical equation systems were solved after applying Lagrange formulation for each element.

Most of the work has focused on numerical methods such as methods integration step-by-step in time to solve the equations of the movement. These methods proved to be well adapted to the linear equations at periodic coefficients. The most commonly used time method is the

implicit method of Newmark for its numerical stability and computation time ratio—interesting precision for industrial applications [26]. However, it requires a judicious choice of integration parameters and initial conditions. The solution is given in the field time; the transition to the frequency domain is performed by a Fourier transform of the response. This method is suitable for this work. Newmark's algorithm is presented from the following linear equilibrium equation:

$$\boldsymbol{M}\ddot{\boldsymbol{q}} + \boldsymbol{C}\dot{\boldsymbol{q}} + (\boldsymbol{K_b} + \boldsymbol{K_e}(\boldsymbol{t}))\boldsymbol{q} = \boldsymbol{F}(\boldsymbol{t}). \tag{7}$$

It is worth noting that q represents the global coordinates of the two planetary gears.

$$\boldsymbol{q} = [\boldsymbol{q_r}, \boldsymbol{q_t}]. \tag{8}$$

The $\boldsymbol{q_r}$ and $\boldsymbol{q_t}$, present, respectively, the reaction and test gear DOF.

$\boldsymbol{M}$ is the mass matrix, $\boldsymbol{C}$ presents the damping matrix, $\boldsymbol{K_b}$ is the bearings matrix, $\boldsymbol{K_e}(\boldsymbol{t})$ is the time-varying stiffness matrix and $\boldsymbol{F}(\boldsymbol{t})$ presents the external force vector applied to the system.

$\boldsymbol{K_e}(\boldsymbol{t})$ is formulated as a summation of a stiffness matrix $\boldsymbol{K}$ and the time-varying matrix $\boldsymbol{k}(\boldsymbol{t})$ defined in [22].

q is the DOF vector defined as:

$$q = \begin{Bmatrix} q_r \\ q_t \end{Bmatrix} \tag{9}$$

$$\begin{aligned} q_r = \{&U_{cr}, V_{cr}, W_{cr}, \rho_{cxr}, \rho_{cyr}, \rho_{czr}, U_{rr}, V_{rr}, W_{rr}, \rho_{rxr}, \rho_{ryr}, \rho_{rzr}, U_{sr}, V_{sr}, W_{sr}, \\ &\rho_{sxr}, \rho_{syr}, \rho_{szr}, U_{1r}, V_{1r}, W_{1r}, \rho_{1xr}, \rho_{1yr}, \rho_{1zr}, U_{2r}, V_{2r}, W_{2r}, \rho_{2xr}, \rho_{2yr}, \rho_{2zr}, \\ &U_{3r}, V_{3r}, W_{3r}, \rho_{3xr}, \rho_{3yr}, \rho_{3zr}\} \end{aligned} \tag{10}$$

$$\begin{aligned} q_t = \{&U_{ct}, V_{ct}, W_{ct}, \rho_{cxt}, \rho_{cyt}, \rho_{czt}, U_{rt}, V_{rt}, W_{rt}, \rho_{rxt}, \rho_{ryt}, \rho_{rzt}, U_{st}, V_{st}, W_{st}, \\ &\rho_{sxt}, \rho_{syt}, \rho_{szt}, U_{1t}, V_{1t}, W_{1t}, \rho_{1xt}, \rho_{1yt}, \rho_{3zt}, U_{2t}, V_{2t}, W_{2rt}, \rho_{2xt}, \rho_{2yt}, \rho_{2zt}, \\ &U_{3t}, V_{3t}, W_{3t}, \rho_{3xt}, \rho_{3yt}, \rho_{3zt}\} \end{aligned} \tag{11}$$

$\boldsymbol{M}$ denotes the mass matrix, $\boldsymbol{K_b}$ is the bearing and shaft stiffness matrix, $\boldsymbol{K_e}(\boldsymbol{t})$ is the time-varying stiffness matrix and $\boldsymbol{F}(\boldsymbol{t})$ stands for the external force vector applied to the system.

$$F(t) = \left[\frac{T_{cr}}{r_{cr}}, \frac{T_{rr}}{r_{rr}}, \frac{T_{sr}}{r_{sr}}, 0, 0, 0, \frac{T_{ct}}{r_{ct}}, \frac{T_{rt}}{r_{rt}}, \frac{T_{st}}{r_{st}}, 0, 0, 0\right] \tag{12}$$

T_{cr}, T_{rr}, T_{sr}, T_{ct}, T_{rt}, T_{st} are the external torques applied respectively in the reaction carrier, the reaction ring, the reaction sun, the test carrier, the test ring and the test sun.

The damping matrix C is given by:

$$C = \alpha M + \beta K, \tag{13}$$

where α and β are two constants [26].

All matrices are presented in what follows:

$$M = \begin{bmatrix} M_t & 0 \\ 0 & M_r \end{bmatrix} \tag{14}$$

$$M_i = \begin{bmatrix} M_c & 0 & 0 & 0 & 0 & 0 \\ 0 & M_r & 0 & 0 & 0 & 0 \\ 0 & 0 & M_s & 0 & 0 & 0 \\ 0 & 0 & 0 & M_1 & 0 & 0 \\ 0 & 0 & 0 & 0 & M_2 & 0 \\ 0 & 0 & 0 & 0 & 0 & M_3 \end{bmatrix} \quad i = t, r \tag{15}$$

Table 1. Bearing stiffness

	Sun	Planet (3)	Ring	Carrier
K_{bx} (N/m)	1.5×10^{8}	1.1×10^{8}	8×10^{8}	1×10^{8}
K_{by} (N/m)	1.5×10^{8}	1.1×10^{8}	8×10^{8}	1×10^{8}
K_{bz} (N/m)	1.1×10^{8}	3×10^{8}	1×10^{8}	5×10^{8}
$K_{b\Phi}$ (N·m/rad)	6×10^{9}	6×10^{9}	1.5×10^{9}	6×10^{9}
$K_{b\Psi}$ (N·m/rad)	6×10^{9}	6×10^{9}	1.5×10^{9}	6×10^{9}
$K_{b\theta}$ (N·m/rad)	1×10^{-3}	1×10^{-3}	8×10^{10}	1×10^{-3}

Table 2. Shaft parameters

	Flexural (N/m)	Torsional (N·m/rad)	Tractional (N/m)
Sun	4.9×10^{5}	3.73×10^{4}	4.85×10^{8}
Carrier	1.1×10^{7}	8.38×10^{5}	1.25×10^{9}

$$M_{ij}=\begin{bmatrix} m_j & 0 & 0 & 0 & 0 & 0\\ 0 & m_j & 0 & 0 & 0 & 0\\ 0 & 0 & m_j & 0 & 0 & 0\\ 0 & 0 & 0 & \frac{I_j}{r^2{}_j} & 0 & 0\\ 0 & 0 & 0 & 0 & \frac{I_j}{r^2{}_j} & 0\\ 0 & 0 & 0 & 0 & 0 & \frac{2*I_j}{r^2{}_j} \end{bmatrix} \quad j=c,r,s,1,2,3 \tag{16}$$

The bearing stiffness matrix K_b

$$K_b=\mathrm{diag}(K_{cr},K_{rr},K_{sr},K_{1r},K_{2r},K_{3r},K_{ct},K_{rt},K_{st},K_{1t},K_{2t},K_{3t}) \tag{17}$$

$$K_{ij}=\mathrm{diag}(K_{ijx},K_{ijy},K_{ijz,}K_{ij^{\delta}},K_{ij^{\varphi}},K_{ij\chi}) \quad i=c,r,s, \tag{18}$$

$$K_{kjb}=\mathrm{diag}(K_{kjb},K_{kjb},K_{kjb},K_{k^{\delta}},K_{kj^{\varphi}},0) \quad k=1,2,3 \quad j=r, \tag{19}$$

$$\psi_r=\alpha_i+\alpha_r \tag{20}$$

$$\psi_s=\alpha_i-\alpha_s \tag{21}$$

The stiffness matrix K_m:

$$K_m=\begin{bmatrix} K_{mr} & 0\\ 0 & K_{mt}\end{bmatrix}+K_c \tag{22}$$

$$K_m=\begin{bmatrix} \sum K_{c1}^{n} & 0 & 0 & K_{c2}^{1} & K_{c2}^{2} & K_{c2}^{3}\\ 0 & \sum K_{r1}^{n} & 0 & K_{r2}^{1} & K_{r2}^{2} & K_{r2}^{2}\\ 0 & 0 & \sum K_{s1}^{n} & K_{s2}^{1} & K_{s2}^{2} & K_{s2}^{3}\\ K_{c2}^{1} & K_{r2}^{1} & K_{s2}^{1} & K_{PP}^{1} & 0 & 0\\ K_{c2}^{2} & K_{r2}^{2} & K_{s2}^{2} & 0 & K_{PP}^{2} & 0\\ K_{c2}^{3} & K_{r2}^{3} & K_{s2}^{3} & 0 & 0 & K_{PP}^{3}\end{bmatrix} \tag{23}$$

All these matrices are presented in the appendix of [22] and Tables 1 and 2 list the values of the different parameters.

Based on the approximate average MSF predictions ($\approx 3.0\times10^{8}$ N/m) in case of static loading condition [27], the stiffness of bearing components are estimated (Table 1). The shaft stiffness was computed analytically using a theoretical formula.

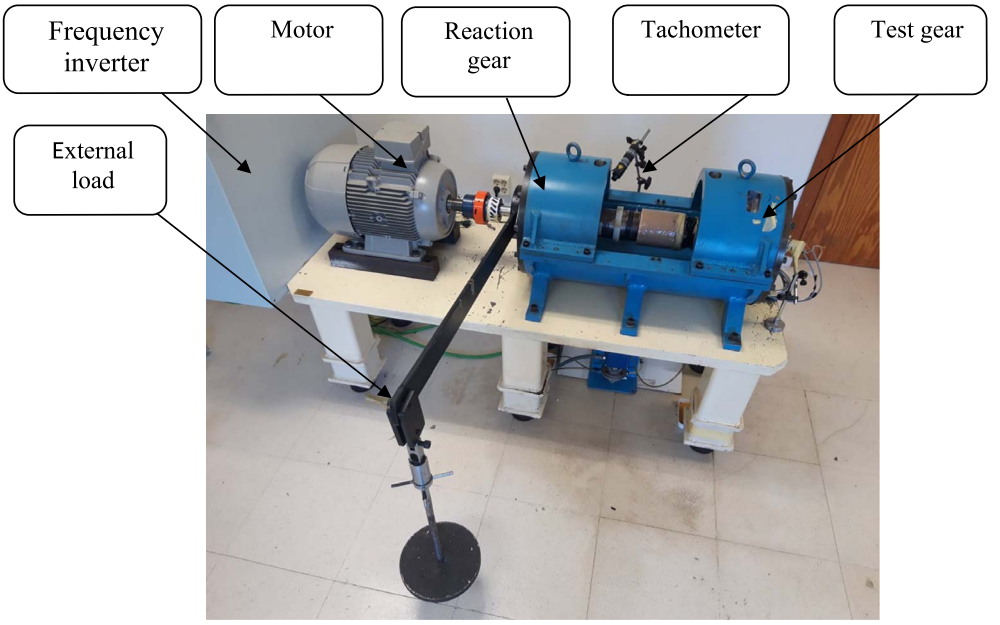

Figure 3. Test rig.

Table 3. Test bench basic dimensions

	Ring	Planets	Sun	Carrier
Teeth number	65	24	6	–
Mass (kg)	28.1	1.22	0.48	3.64
Moment of inertia (kg·m^2)	7×10^{-4}	2×10^{-3}	3.5×10^{-4}	2×10^{-4}
Base diameters (mm)	249.4	92.1	61.4	0.17
Tip diameters (mm)	257.9	100.6	69.9	0.18
Pressure angle (°)			20	
Module (mm)			4	

5. Experimental test rig

The analytical equation systems are solved after applying Lagrange formulation for each element.

This study aims to collect the vibration data using planetary gear with power recirculation test bench. The principal elements of this test bench are displayed in Figure 3. It includes two planetary gear sets mounted back-to-back allowing the energy recirculation, as used in different research studies [22, 27, 28].

Four tri-axial accelerometers (ENDEVCO/65M-100/10023) with high sensitivity (101.6 MV/g on x direction, 103 MV/g on y direction and 101.9 MV/g on z direction) were used. These were fixed on the reaction gear set and the test ring to measure the instantaneous accelerations. To measure the angular accelerations, sensors were mounted in the tangential direction of the ring (ρ_{rzt} DOF).

A LED tachometer was used to measure the input speed and a zebra pattern surface was mounted on the input shaft.

Table 3 displays the basic dimensions of the bench.

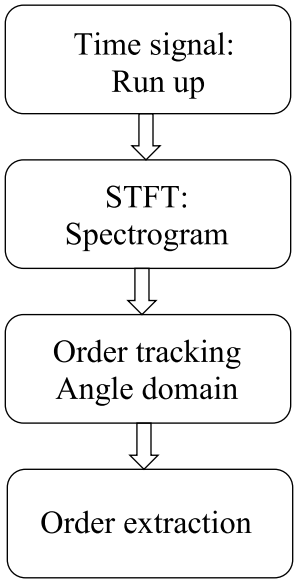

Figure 4. Signal processing steps.

The two-stage planetary gears were driven by an electric motor connected to the two-gear set through an elastic coupling. The motor is controlled using Starter software with the help of a frequency inverter "MICROMASTER 440".

6. Results and discussion

The results are presented as shown in the flowchart given in Figure 4: during each step, the results obtained from the experimental and numerical tests were compared to each other.

6.1. *Torque influence on the dynamic behaviour*

During the run-up regime, the input speed has a ramp shape between 0 and 1000 rpm for both experimental and numerical cases (Figure 5).

The simulation and experimental tests are carried out during run-up regime for four torque cases (200 N·m, 400 N·m, 600 N·m and 800 N·m).

The rotation of the reaction ring is free, allowing the introduction of an external load to the test bench. To this end, the rigid arm where the masses were introduced, was attached to the reaction ring. Consequently, the inertia and mass of the reaction ring varied with the load as illustrated in Table 4.

The MSF was obtained using Hertzian contact theory and finite element method. The procedure given by Del Rincón *et al.* [29], was divided into three steps. Firstly, the tooth geometry was defined, and the location of the contact points was computed by considering the analytic formulation of the involute–involute contact. Then, two phenomena were considered: (i) the nonlinear local deformations near the contact area where an analytical nonlinear formulation of Hertzian type for local deflections was used, (ii) the tooth body deflections due to linear bending, shearing and compression was analysed. Two-dimensional finite element model of teeth in contact was achieved.

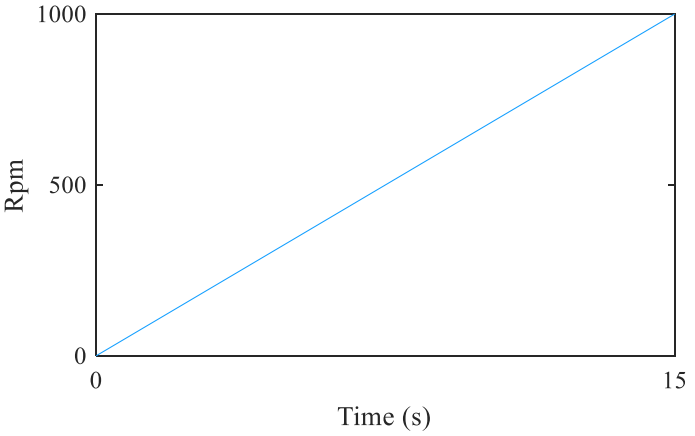

Figure 5. Input rotational speed.

Table 4. Parameters varied with the load

Load (N·m)	Inertia of reaction ring (kg·m^2)	Mass of reaction ring (kg)	Average of sun planets mesh stiffness (N/m)	Average of ring planets mesh stiffness (N/m)
200	0.7479	38.1	4.04×10^8	5.84×10^8
400	1.0588	48.1	4.14×10^8	6.07×10^8
600	1.3698	58.1	4.23×10^8	6.27×10^8
800	1.6807	68.1	4.42×10^8	6.69×10^8

These functions are loaded dependently, their amplitude increases when the loads increase through the increase of the contact area between the teeth. Table 4 shows the applied loads that impact the different parameters of the system.

During the run-up regime, the MSF period decreases as the speed increases [30,31]. The trend of these functions is shown in the Figure 6. The mesh phasing too was considered.

The acceleration signals on the fixed ring are displayed in Figures 7 and 8. These figures show that the vibration and oscillation amplitudes increase respectively with time. All accelerations are shown in the radial direction.

However, in the run-up regime, the MSF which is the principal source of excitation of the system is characterised by non-constant period. The acceleration issued from the numerical model was compared to the experimental response as illustrated in Figures 7 and 8.

In Figures 7 and 8, it is noticeable that the acceleration and input torque amplitudes are both directly proportional and increase because of the deformation increase at the teeth and the bearing owing to the increase in effort. Also, the MSF and the period of teeth in contact (Figure 6) varied too; this variation is due to the sensitivity of the Hertzian contact to the load [29]. This phenomenon leads to the system instability presented by the high vibration. Also, critical scenarios could occur when the system is overloaded [32].

Hence a time–frequency presentation STFT was used to analyse the GMF evolution in time. It is clear from Figures 9 and 10 that the GMF amplitude increases with torque. This is due to the presence of interesting energy in the spectrograms along the frequency bandwidth indicating an excitation of structural resonances. Also, two kinds of lines are noticed: oblique lines from left to right due to the evolution of the GMF function and its harmonics and vertical lines explained by the presence of some natural frequencies.

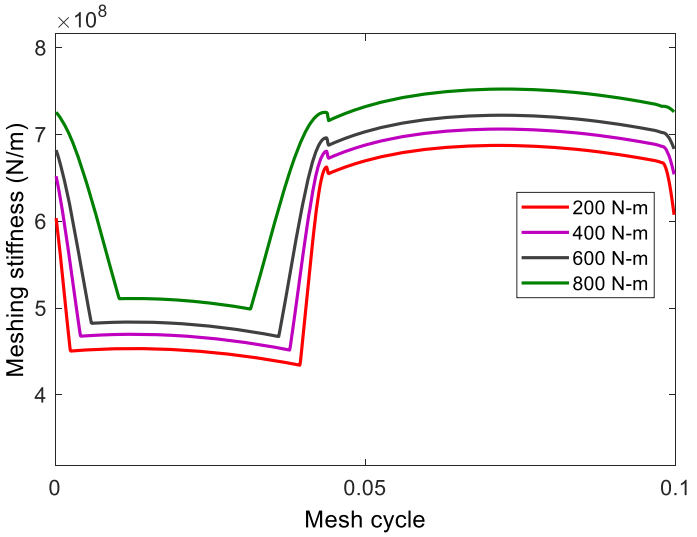

Figure 6. Ring-planets MSF trend.

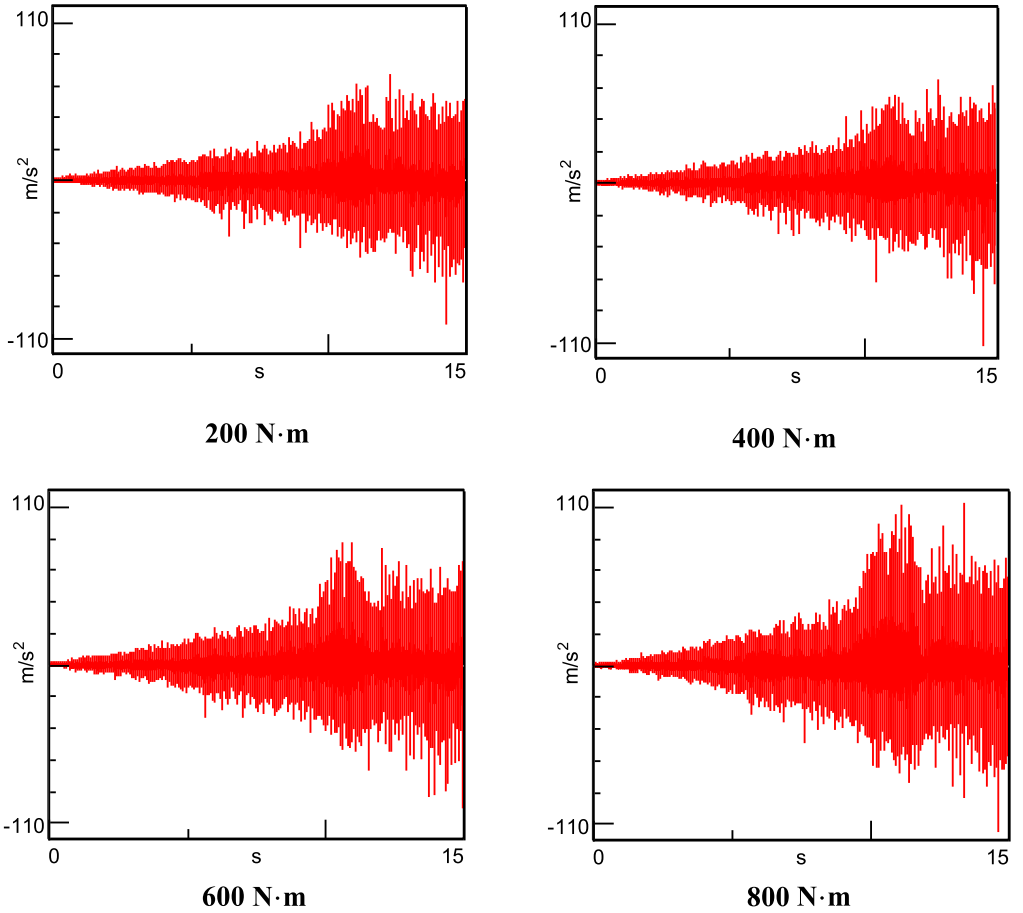

Figure 7. Measured acceleration on the fixed ring at ρ_{rzt} degree of freedom.

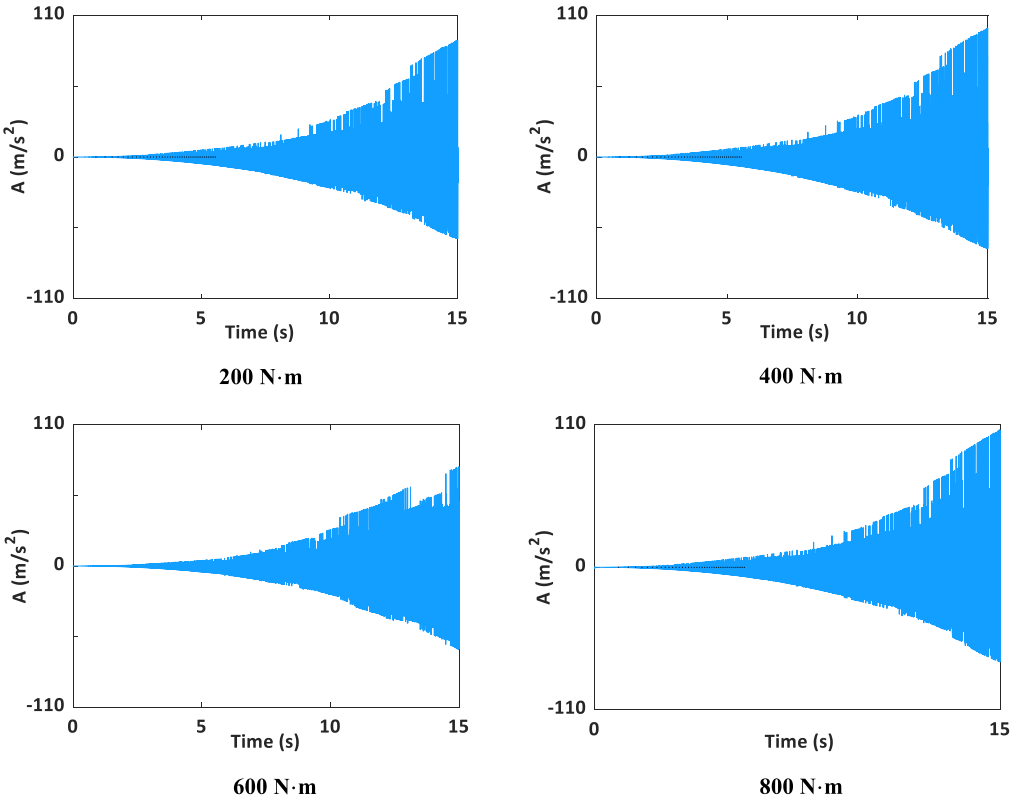

Figure 8. Simulated acceleration on the fixed ring at ρ_{rzt} DOF.

6.2. *Torque influence on modal properties*

After studying the influence of the torque on vibration response and analysing the dynamic behaviour of the system in different loading conditions, the torque influence on MP was highlighted using the OBMA. This method allows the identification of MP when the excited system is in non-stationary condition.

6.2.1. *Order tracking*

After extracting the time signal and plotting the time–frequency map (Figure 11), the OT presented on the angular domain was investigated.

According to the map order, different order functions can be extracted. These functions are computed according to the map order because the OBMA uses the order functions as input data to identify the MP. In the studied cases the order 64.4 was selected to identify the MP in frequency bandwidth (0–1000 Hz), (Figures 12 and 13).

The order functions are sensitive to the load too; their amplitude increases with the increase in load.

6.2.2. *Natural frequencies and damping identification*

In this subsection, the OBMA techniques were applied. In this case, the order functions are the transfer functions.

By using a stabilization diagram which used order function (Figures 12 and 13) as input data, the natural frequencies and modal damping were estimated as displayed in Table 5 and is illustrated in Figure 14.

Table 5. Natural frequencies and modal damping for different applied loads

Mode	200 N·m				400 N·m				600 N·m				800 N·m			
	Num (Hz)	Exp (Hz)	Error (%)	Damping (%)	Num (Hz)	Exp (Hz)	Error (%)	Damping (%)	Num (Hz)	Exp (Hz)	Error (%)	Damping (%)	Num (Hz)	Exp (Hz)	Error (%)	Damping (%)
1	66	72	8.3	3.2	67	73	8.21	4.75	67	77	12.9	5.45	67	78	14.1	6.92
2	115	125	8	3.6	117	130	10.0	4.62	118	131	9.92	5.62	120	135	11.1	6.95
3	150	159	5.66	3.3	152	167	8.98	4.33	155	167	7.18	5.33	158	169	6.50	6.82
4	184	191	3.6	3.7	185	195	5.12	4.4	187	196	4.59	5.97	190	199	4.52	6.14
5	243	250	2.8	3	246	252	2.38	4.57	249	252	1.19	5.12	250	255	1.96	6.86
6	285	294	3.06	3.41	287	297	3.36	4.06	289	299	3.34	5.86	292	302	3.31	6.44
7	317	325	2.46	3.13	317	325	2.46	4.02	319	326	2.14	5.49	322	329	2.12	6.05
8	351	354	0.84	3.5	352	357	1.40	4.86	353	360	1.94	5.14	355	362	1.93	6.64
9	366	375	2.4	3.76	368	377	2.38	4.88	369	379	2.63	5.32	372	380	2.10	6.97
10	–	383	–	2.9	–	385	–	3.3	–	388	–	3.8	–	390	–	4.3
11	399	404	1.23	3.7	400	407	1.71	4.67	402	410	1.95	5.11	405	413	1.93	6.39
12	435	441	1.36	3.29	437	443	1.35	4.29	439	445	1.34	5.29	441	447	1.34	6.29
13	466	471	1.06	3.15	469	473	0.84	4.15	471	477	1.25	5.15	473	479	1.25	6.15
14	514	521	1.34	3.41	515	530	2.83	4.41	518	534	2.99	5,41	522	535	2.42	6.41

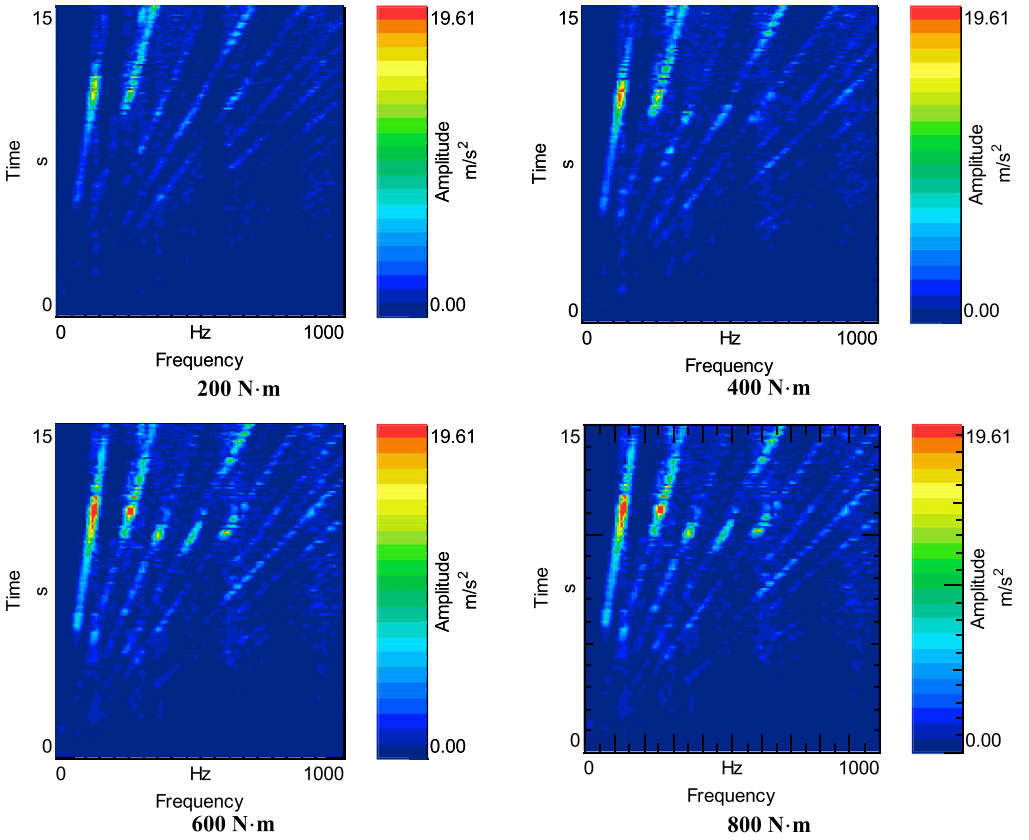

Figure 9. Measured STFT on the fixed ring at ρ_{rzt} DOF.

According to the analysis illustrated in Figure 14(a), it is noticeable that the presented parameters are sensitive to load variation. The increase in torque has effects on the MSF amplitude. In fact, the contact area between the teeth increases, producing a variation in both fillet stiffness and the Hertzian one [33]. In addition, the entire system matrices change. However, (Figure 14(b)) illustrates the frequency errors between the identified modes. So, we believe that the observed errors are due to several factors such as the modelling of the bearing components as isotropic or the effects of accumulation of vibration paths on the ring [34]. Also, this behaviour is an issue of the MSF variation on the MP [21]. For the modal damping, an interesting result is presented as shown in (Figure 14(c)). We notice that with increasing torque, the damping values too increase. This information is very important in the case of rotating machinery applications, the input load has an influence on critical parameters of the structure such as the natural frequency and the damping. For design purpose, we should consider this phenomenon. This is so mainly due to the effect of the width of the film oil and the contact friction between teeth, especially in non-stationary regimes [35].

The results obtained show interesting findings; in fact, the impact of load on the natural properties of the system should be carefully studied, as we know that these kinds of system are usually subjected to various and important external excitations like the external load. The load transmitted to all the components encounters several influencing functions and parameters. As mentioned, the load impacts on the meshing functions. In fact, in the model we have considered only this parameter, but in reality, the load can introduce such parameters which are linked to

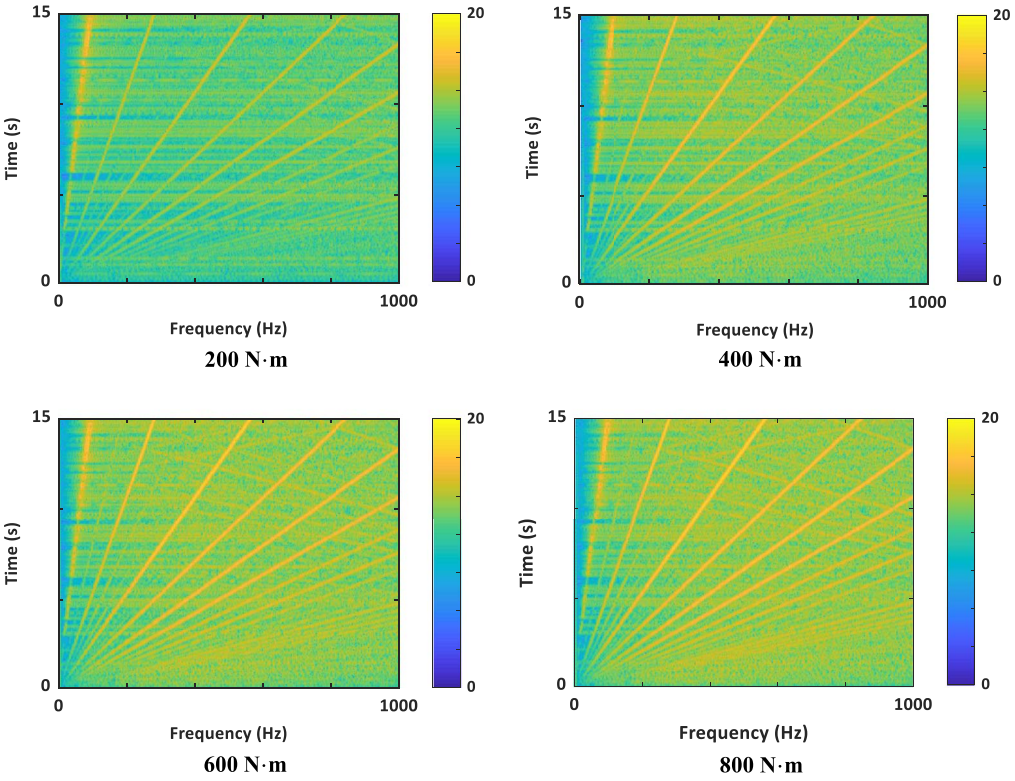

Figure 10. Simulated STFT on the fixed ring at ρ_{rzt} DOF.

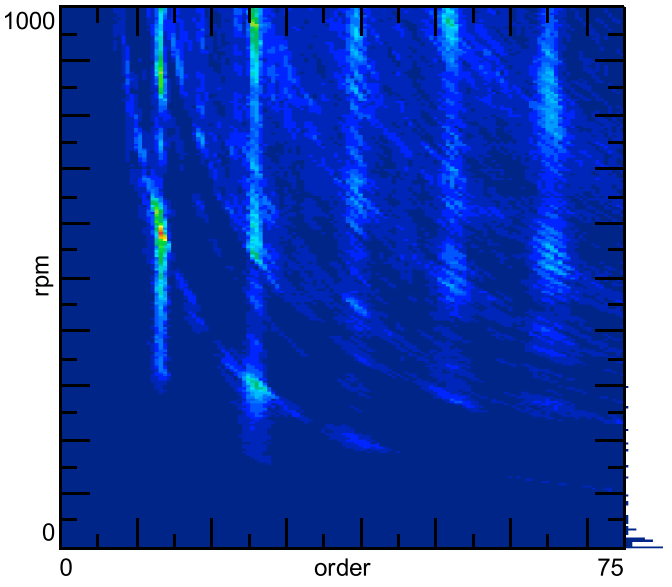

Figure 11. Order map.

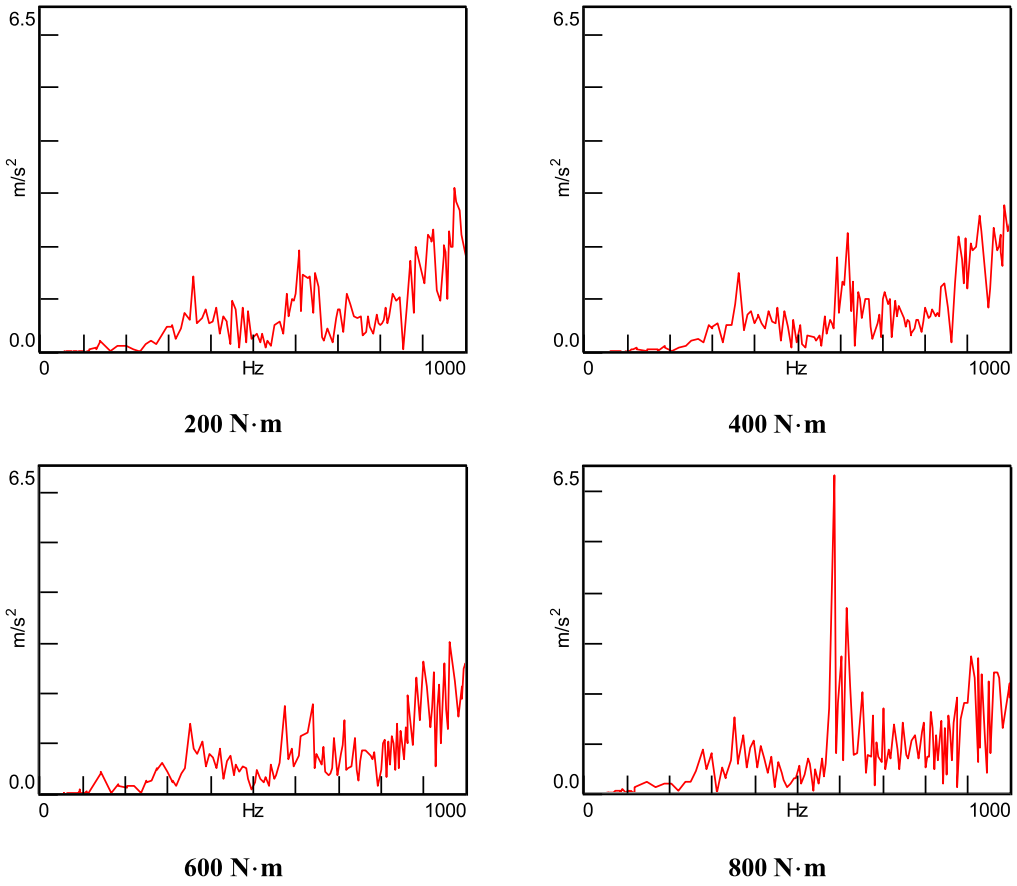

Figure 12. Measured order on the fixed ring at ρ_{rzt} DOF.

the system and which can as well modify the modal parameter. In fact, when the load increases, the contact between teeth increases, so that friction contact i.e., the friction force increases and is modified. This phenomenon is not considered in the model but it exists in reality, and especially in our case, it has great importance, because as the system starts running with different levels of load, it causes a high friction load. This phenomenon was examined by many researchers, who studied its impact on the dynamic vibration response. Certainly, in the work of Liu *et al.* [36], the MP of planetary gear system considering the friction contact is investigated, and the authors show that the friction coefficient has great influence on the natural frequency. Due to the asymmetry of the stiffness matrix containing the friction coefficient, in the elastic-discrete system complex conjugate eigenvalues and eigenvectors appear.

Another parameter which is suppressed but which has a very important influence on dynamic response as well as system modal behaviour is the nature of the ring components. The ring gear which is generally the stationary element in the epicyclic gear system experiences elastic deformation, and the ring component is generally modelled as a rigid body, just as the same for the other components. In such an application where the external speed is very high and the transmitted load is high, a deformation can be led on to these components, this deformation then automatically generates instability on the system as well as on the system vibration response as well as on the modal parameters. This phenomenon was also neglected in the developed model

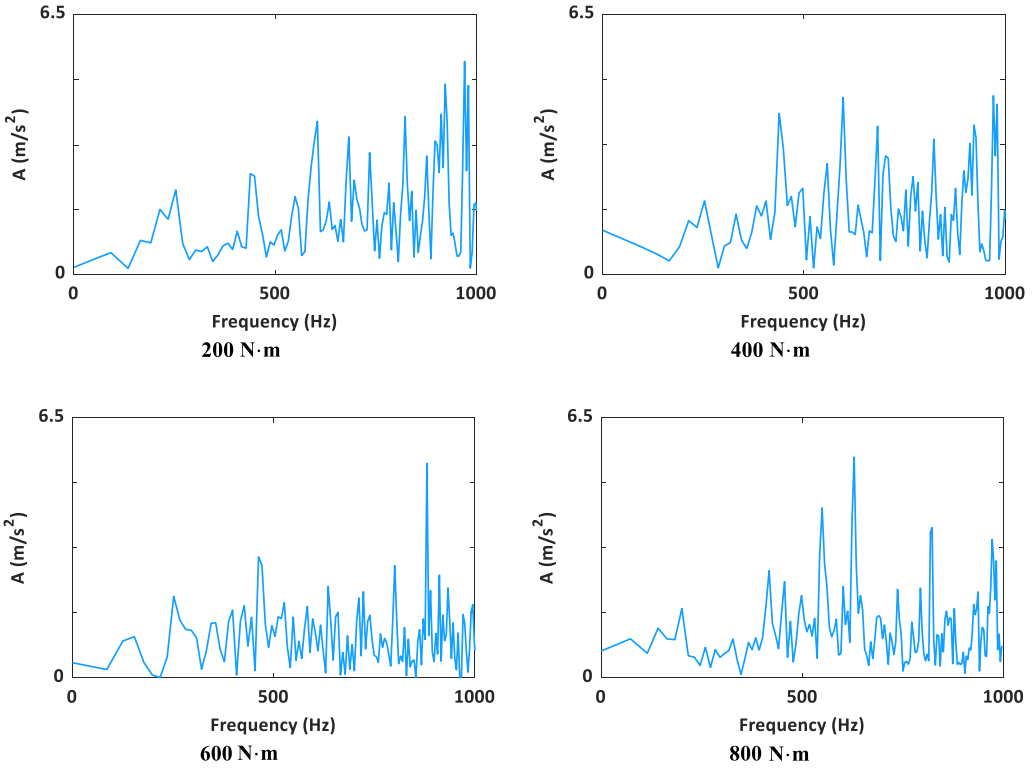

Figure 13. Simulated order on the fixed ring at ρ_{rzt} DOF.

but can be presented experimentally. The bench was subjected to various research investigations and was exploited in over many years, so that the variation of load on modal parameters was transmitted, and aided in the ring deformation. This phenomenon was confirmed by Wang and Parker [37].

In fact, planetary gear transmissions are a very complex system, they cluster several functions and parameters, whether geometrical kinematical or dynamical. It could also be mentioned that mesh phasing parameter has an influence on modal response [38], the defect of floating sun which is generally presented in planetary gear transmission can lead to an instability. So also, the bearing element, the load sharing and the oil film.

7. Conclusion

OMA using order-based techniques is applied on two-stage planetary gear transmissions. The proposed method shows a significant result which can be relevant in many practical cases. A series of measurements, tests and simulations were established to understand this method and to highlight the influence of the load on the MP at the same time. The experiments were performed on test bench and the three-dimensional lumped model was developed to achieve further insight into the dynamic behaviour of the system. In the first step, the dynamic behaviour of the system was investigated for different load conditions. This proved that the amplitude of the internal forces and the period of double contact increases by the evolution of the torque. Consequently, both the ring inertia and the MSF average value change. This behaviour was reflected in the MSF trends through a variation in the amplitude of acceleration. The time–frequency map was

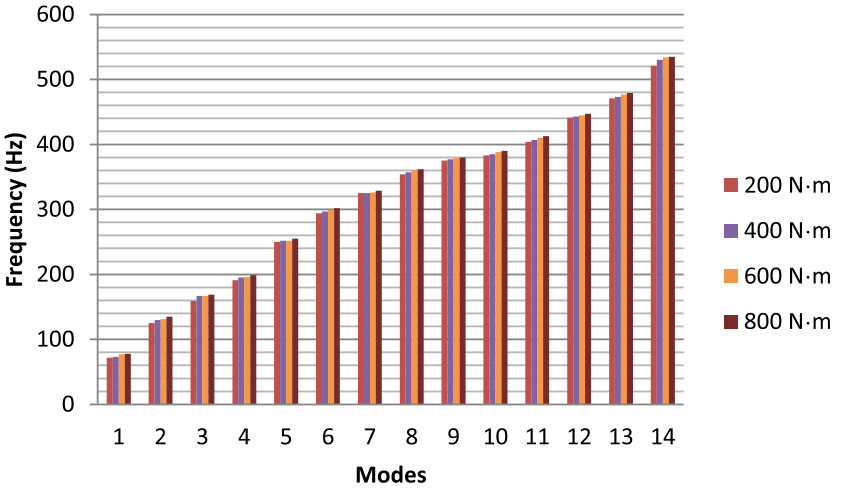

(a)

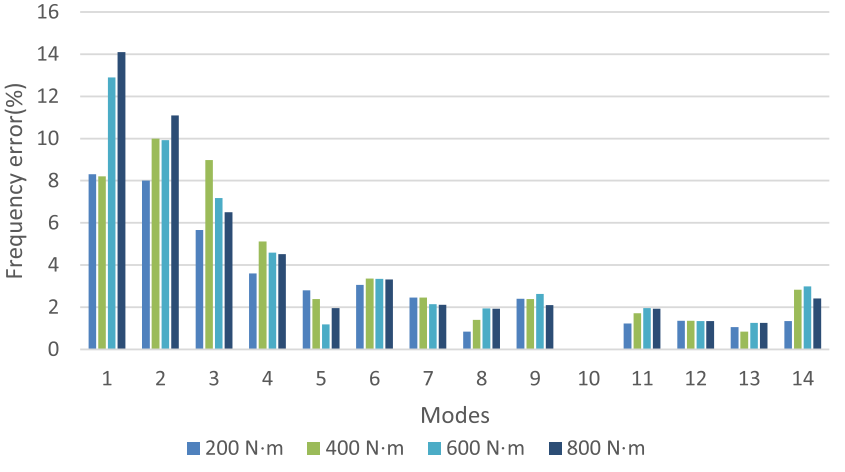

(b)

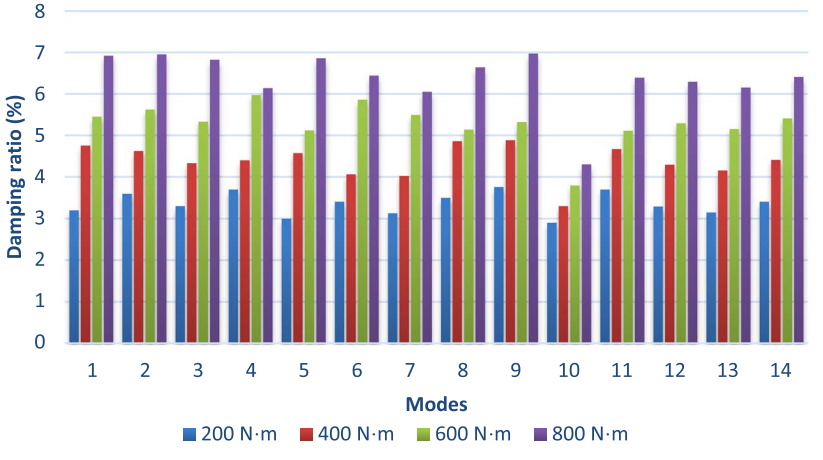

(c)

Figure 14. Torque impact on (a) natural frequency (b) frequency error (c) damping.

determined to evaluate the GMF evolution. In addition, the spectral density related to the first GMF was shown to move to second GMF. This is explained by the fact that when the level of torque varies, the contact area between the teeth increases producing an effective modification in internal force values at the bearing and the teeth components. In fact, this phenomenon introduces a fluctuation in the angle of pressure and consequently an increase in the contact ratio. In a second step, the torque impact on the MP was studied; the angle-domain OT method was developed and compared to experimental results.

The stabilization diagram was then used to analyse and estimate the natural frequencies and the system modal damping. In the case of MP identification, it was found that the MP changed significantly with the load.

With the load increase, the natural frequencies and modal damping significantly change. When the readjustments of the varying load were introduced, the contact between the teeth increased. Thus, it increases the MSF as well as the effort at the bearing and teeth.

Finally, more investigations on mode shapes will be considered in the future work.

Nomenclature

M	Mass matrix
C	Damping matrix
K_B	Bearing matrix
$F(t)$	External force vector
$K_e(t)$	Time-varying stiffness matrix
K	Stiffness matrix
$k(t)$	Time-varying matrix
Q	Vector degree of freedom
m_{ij}	Mass of component i of gear sets j
I_{ij}	Inertia of component i of gear sets j
K_{bix}	Bearing stiffness of the components i in x direction
K_{biy}	Bearing stiffness of the components i in y direction
K_{biz}	Bearing stiffness of the components i in z direction
$K_{bi\Phi}$	Bearing stiffness of the components i in Φ direction
$K_{bi\Psi}$	Bearing stiffness of the components i in Ψ direction
$K_{bi\theta}$	Bearing stiffness of the components i in θ direction
K_{rpi}	Mesh stiffness function between the ring and the planet i ($i = 1,2,3$)
K_{spi}	Mesh stiffness function between the sun and the planet i ($i = 1,2,3$)

Notation

MP	Modal Properties
OMA	Operational Modal Analysis
OT	Order Tracking
RLS	Recursive Least-Squares
OBMA	Order-Based Modal Analysis
MSF	Mesh Stiffness Function
DOF	Degree of Freedom
STFT	Short Time Fourier Transform
GMF	Gear Mesh Frequency

Conflicts of interest

Authors have no conflict of interest to declare.

Acknowledgements

The authors would like to acknowledge the support of the Project DPI2017-85390-P funded by the Spanish Ministry of Economy, Industry, and Competitiveness to this research.

References

[1] D. Z. Veljkovic, I. Macuzic, B. Jeremic, P. Mijovic, P. M. Todorovic, "Investigation on the RLS and Kalman based adaptive order tracking techniques for rotating machinery analysis", *Chem. Eng. Trans.* **33** (2013), p. 25-30.

[2] A. Hammami, A. F. Del Rincon, F. V. Rueda, F. Chaari, M. Haddar, "Modal analysis of back-to-back planetary gear: experiments and correlation against lumped-parameter model", *J. Theor. Appl. Mech.* **53** (2015), p. 125-138.

[3] T. M. Ericson, R. G. Parker, "Planetary gear modal vibration experiments and correlation against lumped-parameter and finite element models", *J. Sound Vib.* **332** (2013), no. 9, p. 2350-2375.

[4] A. Mbarek, A. F. Del Rincon, A. Hammami, M. Iglesias, F. Chaari, F. Viadero, M. Haddar, "Comparison of experimental and operational modal analysis on a back-to-back planetary gear", *Mech. Mach. Theory* **124** (2018), p. 226-247.

[5] I. Bucher, D. J. Ewins, "Modal analysis and testing of rotating structures", *Phil. Trans. R. Soc. Lond. A* **359** (2001), p. 61-96.

[6] R. Provasi, G. A. Zanetta, A. Vania, "The extended Kalman filter in the frequency domain for the identification of mechanical structures excited by sinusoidal multiple inputs", *Mech. Syst. Signal Process* **14** (2000), no. 3, p. 327-341.

[7] P. Mohanty, D. J. Rixen, "A modified Ibrahim time domain algorithm for operational modal analysis including harmonic excitation", *J. Sound Vib.* **275** (2004), p. 375-390.

[8] P. Mohanty, D. J. Rixen, "Modified SSTD method to account for harmonic excitations during operational modal analysis", *Mech. Mach. Theory* **39** (2004), p. 1247-1255.

[9] P. Mohanty, D. J. Rixen, "Operational modal analysis in the presence of harmonic excitation", *J. Sound Vib.* **270** (2004), p. 93-109.

[10] P. Mohanty, D. J. Rixen, "Modified ERA method for operational modal analysis in the presence of harmonic excitations", *Mech. Syst. Signal Process* **20** (2006), p. 114-130.

[11] S. H. Kordkheili, S. M. Massouleh, S. Hajirezayi, H. Bahai, "Experimental identification of closely spaced modes using NExT-ERA", *J. Sound Vib.* **412** (2018), p. 116-129.

[12] S. V. Modak, C. Rawal, T. K. Kundra, "Harmonic elimination algorithm for operational modal analysis using random decrement technique", *Mech. Syst. Signal Process* **24** (2010), p. 922-944.

[13] S. V. Modak, "Separation of structural modes and harmonic frequencies in operational modal analysis using random decrement", *Mech. Syst. Signal Process* **41** (2013), p. 366-379.

[14] B. Peeters, H. Van der Auweraer, P. Guillaume, J. Leuridan, "The PolyMAX frequency-domain method: a new standard for modal parameter estimation", *Shock Vib.* **11** (2004), no. 3-4, p. 395-409.

[15] S. Haykin, *Adaptive Filter Theory*, Prentice-Hall, Englewood Cliffs, NJ, 1986.

[16] J. Leuridan, G. E. Kopp, N. Moshrefi, H. Vold, "High resolution order tracking using Kalman tracking filters – theory and applications", in *Proceedings of Noise and Vibration Conference*, 1995, SAE Technical Paper 951332.

[17] H. Herlufsen, S. Gade, H. Konstantin-Hansen, H. Vold, "Characteristics of the Vold/Kalman order tracking filter", in *Proceedings of 17th Annual International Modal Analysis Conference*, 1999.

[18] H. Vold, J. Deel, "Vold–Kalman order tracking: new methods for vehicle sound quality and drivetrain NVH applications", in *Proceedings of G50 Noise and Vibration Conference*, 1997, SAE Technical Paper 972033.

[19] J. D. Wu, C. W. Huang, J. C. Chen, "An order-tracking technique for the diagnosis of faults in rotating machineries using a variable step-size affine projection algorithm", *NDT&E Int.* **38** (2005), p. 119-127.

[20] M. Yang, Y. Dai, Q. Huang *et al.*, "A modal parameter identification method of machine tools based on particle swarm optimization", *Proc. Inst. Mech. Eng., Part C* **233** (2019), no. 17, p. 6112-6123.

[21] T. M. Ericson, R. G. Parker, "Experimental measurement of the effects of torque on the dynamic behavior and system parameters of planetary gears", *Mech. Mach. Theory* **74** (2014), p. 370-389.

[22] A. Mbarek, A. Hammami, A. F. Del Rincon, F. Chaari, F. V. Rueda, M. Haddar, "Effect of load and meshing stiffness variation on modal properties of planetary gear", *Appl. Acoust.* **147** (2019), p. 32-43.

[23] A. Hammami, A. Fernandez, F. Chaari, M. Iglesias, F. Viadero, M. Haddar, "Effects of variable loading conditions on the dynamic behavior of planetary gear withpower recirculation", *Measurement* **94** (2016), p. 306-315.

[24] E. Di Lorenzo, S. Manzato, B. Peeters, F. Vanhollebeke, W. Desmet, F. Marulo, "Order-Based Modal Analysis: a modal parameter estimation technique for rotating machineries", in *6th International Operational Modal Analysis Conference Proceedings*, Edicionesunivoviedo, 2015, p. 325-332.

[25] E. Di Lorenzo, S. Manzato, F. Vanhollebeke, S. Goris, B. Peeters, W. Desmet, F. Marulo, "Dynamic characterization of wind turbine gearboxes using Order-Based Modal Analysis", in *Proceedings of International Conference on Noise and Vibration Engineering (ISMA2014) and International Conference on Uncertainty in Structural Dynamics (USD2014)*, Katholiekeunivleuven, dept werktuigkunde, 2014, p. 4349-4362.

[26] G. Dhatt, G. Touzot, E. Lefrançois, *Méthode des Éléments Finis – Une Présentation*, Hermès Science Publications, Paris, France, 2005.

[27] J. Wu, Y. Zi, J. Chen, Z. Zhou, "Fault diagnosis in speed variation conditions via improved tacholess order tracking technique", *Measurement* **137** (2019), p. 604-616.

[28] A. Mbarek, A. Hammami, A. F. Del Rincon, F. Chaari, F. V. Rueda, M. Haddar, "Effect of gravity of carrier on the dynamic behavior of planetary gears", in *International Conference Design and Modelling of Mechanical Systems*, Springer, Cham, 2017, p. 975-983.

[29] A. F. Del Rincon, F. Viadero, M. Iglesias, P. García, A. De-Juan, R. Sancibrian, "A model for the study of meshing stiffness in spur gear transmissions", *Mech. Mach. Theory* **61** (2013), p. 30-58.

[30] F. Viadero, A. Fernández, M. Iglesias, A. De-Juan, E. Liaño, M. A. Serna, "Non-stationary dynamic analysis of a wind turbine power drivetrain: Offshore considerations", *Appl. Acoust.* **77** (2014), p. 204-211.

[31] J. Lin, R. G. Parker, "Parametric Instabilities in Planetary Gears under Mesh Stiffness Variations", *J. Vib. Acoust.* **249** (2000), no. 1, p. 129-146.

[32] R. J. Drago, "The effect of start-up load conditions on gearbox performance and life failure analysis, with supporting case study", in *American Gear Manufacturers Association Fall Technical Meeting*, 2009.

[33] A. Hammami, A. Mbarek, A. Fernández, F. Chaari, F. Viadero, M. Haddar, "Dynamic behavior of the nonlinear planetary gear model in nonstationary conditions", *Proc. Inst. Mech. Eng. Part C* **235** (2021), no. 20, p. 4648-4662.

[34] F. Jiang, K. Ding, G. He, Y. Sun, L. Wang, "Vibration fault features of planetary gear train with cracks under time-varying flexible transfer functions", *Mech. Mach. Theory* **158** (2021), article no. 104237.

[35] A. Diez-Ibarbia, A. Fernandez-del Rincon, P. Garcia, F. Viadero, "Gear rattle dynamics under non-stationary conditions: The lubricant role", *Mech. Mach. Theory* **151** (2020), article no. 103929.

[36] W. Liu, Z. Shuai, Y. Guo, D. Wang, "Modal properties of a two-stage planetary gear system with sliding friction and elastic continuum ring gear", *Mech. Mach. Theory* **135** (2019), p. 251-270.

[37] C. Wang, R. G. Parker, "Modal properties and parametrically excited vibrations of spinning epicyclic/planetary gears with a deformable ring", *J. Sound Vib.* **494** (2021), article no. 115828.

[38] R. G. Parker, J. Lin, *Modeling, Modal Properties, and Mesh Stiffness Variation Instabilities of Planetary Gears*, Department of Mechanical Engineering, Ohio State University, Columbus, 2001.